Eur. Phys. J. Appl. Phys. **43**, 165–172 (2008)
DOI: 10.1051/epjap:2008064

THE EUROPEAN PHYSICAL JOURNAL
APPLIED PHYSICS

Wide frequency range analysis of the electromagnetic emissions of electrical machine for diagnosis*

R. Romary[a], D. Roger, and J.F. Brudny

LSEE-Université d'Artois, Technoparc future, 62400 Béthune, France

Received: 3 July 2007 / Accepted: 25 February 2008
Published online: 30 April 2008 –

Abstract. The paper presents the possibilities to evaluate the health of an electrical machine by analyzing its electromagnetic emissions. Different piece of information can be detected according to the frequency range. First of all, a monitoring system sensitive to the degradation of the turn-to-turn insulation quality of the stator winding is presented; it is based on high frequency electromagnetic emissions. The second part of the paper is based on the medium and low frequency emission analysis. It explains how to detect turn-to-turn short circuits in stator windings or in the excitation coils of synchronous machines.

PACS. 77.22.Jp Dielectric breakdown and space-charge effects – 84.50.+d Electric motors – 84.37.+q Measurements in electric variables

1 Introduction

The external magnetic field existing near an operating electrical machine is a very well-known phenomenon. Many studies deal with the analysis and the modeling of this magnetic field [1,2]. As far as the frequency range is concerned, it can be classified in 3 categories:

- High Frequency (HF) emissions (a few MHz) generated by the resonance linked to turn-to-turn capacitances and inductances.
- Medium Frequency (MF) emissions (a few kHz) produced by:
  - the slotting effect, these signals appear even if the machine is directly supplied by the sinusoidal network;
  - the chopping phenomena in the case of PWM supply.
- Low Frequency (LF) emissions (below 100 Hz) linked to the fundamental frequency of the power supply as well as those depending on the rotation frequency.

Each category is able to bring information about geometric, magnetic, or electrical characteristics of an electrical machine. Moreover, the health of the machine can be evaluated by a non-invasive monitoring system. The aim of the paper is to display the possibilities of machine diagnosis by analyzing the external magnetic field. The full frequency range will be used but the study will consider separately the HF emissions and the LF and MF ones. The first is sensitive to the quality of the stator winding turn-to-turn insulation; the second gives information about a fault occurring in the machine.

2 On-line testing of the turn-to-turn insulation quality

The stator insulation failure mechanism is now well-known; it often begins with a local turn-to-turn breakdown, which creates a supplementary thermal stress and an extension of the damage that may reach the ground wall insulation if it is not detected [3]. For adjustable speed drives, these problems occur more frequently because the turn-to-turn voltage includes spikes that may cause partial discharges (PD), which are at the origin of an early aging [4]. Several classical methods can be used for ground insulation testing [5], but it is more difficult to evaluate the quality of the turn-to-turn insulation which is the only way to detect the very beginning of an insulation problem. Until now, very few methods are available, it is possible to perform an impulse testing on an off-line machine [6] or to follow the PD activity on high voltage working machines [7], or with off-line PD testing systems [8]. No method exists for on-line testing of inverter-fed motors.

This part of the paper presents a new on-line monitoring system able to give information on the quality of the turn-to turn insulation. The new system is based on the indirect measurement of the turn-to-turn capacitance of stator windings and on statistical data obtained from measurements on accelerated aging of specimens made with the same enamelled wire.

* This article has been submitted as part of "IET – Colloquium on Reliability in Electromagnetic Systems", 24 and 25 May 2007, Paris

[a] e-mail: raphael.romary@univ-artois.fr

Article published by EDP Sciences

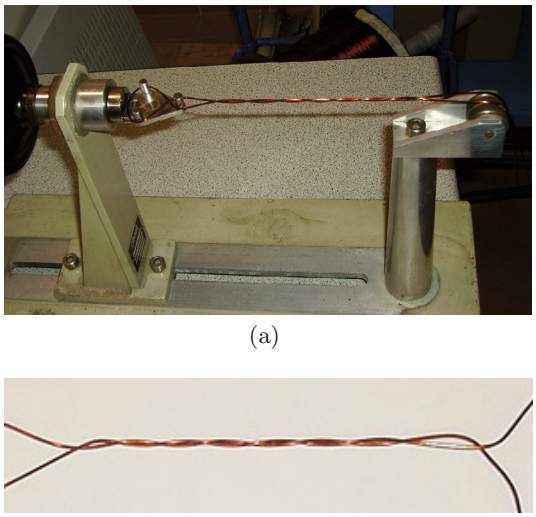

(a)

(b)

Fig. 1. (a) Device used to build the twisted specimens. (b) A standard twisted specimen.

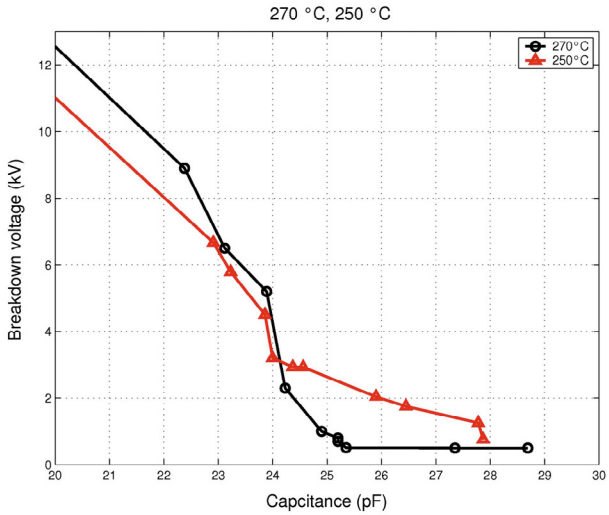

Fig. 2. (Color online) Breakdown voltage versus specimen capacitance.

2.1 Accelerated aging tests

Thermal accelerated aging tests were made using a standard enamelled copper wire, which insulation is made of polyesterimide (THEIC) with an external layer of polyamide-imide; the commercial reference is "Magnebond CAB 200". The tests were performed according to the IEC 60851-5 standard, which specifies totally the procedure. For an enamelled wire whose diameter is 1.25 mm, this standard specifies to make 6 turns with a tensile force of 27 N, using the special device presented in Figure 1a. A resulting twisted specimen is shown in Figure 1b.

A set of 120 specimens was stressed by thermal cycles in order to get an accelerated aging. For 270 °C the cycle time was 60 h and 200 h for a thermal stress of 250 °C. After each cycle, 10 randomly selected specimens were used to measure the breakdown voltage at 50 Hz using the procedure specified by the same IEC standard. The capacitance of each remaining specimen was also measured at 100 kHz with a precision impedance analyzer Agilent 4294 A using the appropriate connection system [9].

As expected, this aging tests show that the breakdown voltage decreases along the test. Another interesting result was also observed for both temperatures: a significant increase of the twisted specimen capacitance. Figure 2 gives a synthesis of experimental results, the vertical axis is the mean value of the breakdown voltages measured after each cycle using the 10 randomly selected specimens. The horizontal axis corresponds to the mean value of capacitance of the remaining specimens. Each point of the curve corresponds to a thermal cycle.

The capacitance measurement, which is a non-destructive test, can be correlated to the specimen breakdown voltage: for the tested enamelled wire, Figure 2 shows that an alert threshold, at about 25 or 26 pF can be defined on this parameter. When the specimen capacitance is higher than this threshold, the breakdown voltage can be considered as "low".

Another set of tests, made with a high frequency and high voltage stresses on the same kind of twisted sample, confirms that the increase of the capacitance can be correlated to the aging of the specimens [10].

During thermal accelerated aging process, 60 identical specimens were added into the oven and submitted, after each thermal cycle, to 400 V–50 Hz during one minute; the result of this test is binary: the specimen insulation fails or not. This test allows computing the cumulative probability of failure at rated voltage [11], which can be expressed with a two parameters Weibull law:

$$F(t) = 1 - \exp\left(-\left(\frac{t}{\eta}\right)^{\beta}\right). \quad (1)$$

With experimental data obtained for 270 °C and 250 °C, the Weibull parameters are respectively $\eta = 574$ h, $\beta = 3.91$ and $\eta = 2275$ h, $\beta = 5.12$. Figure 3 presents the variations of cumulative probabilities of failure versus specimen capacitance for both temperatures. It can be seen that, for a capacitance higher than the same alert threshold situated at about 25 or 26 pF, the specimen cumulative probability of failure at rated voltage cannot be considered as low.

These experimental studies show that the turn-to-turn capacitance variations can be used as an indicator of the winding turn-to-turn insulation aging. A HF lumped parameter model of the machine winding shows that the turn-to-turn capacitance variation have a significant impact on the winding HF resonances [12].

2.2 Turn-to-turn insulation aging monitoring system

The principle of the proposed monitoring system consists in adding a low-level HF voltage to the motor supply in order to measure the variations of the first series resonance.

https://doi.org/10.1051/epjap:2008064 Published online by Cambridge University Press

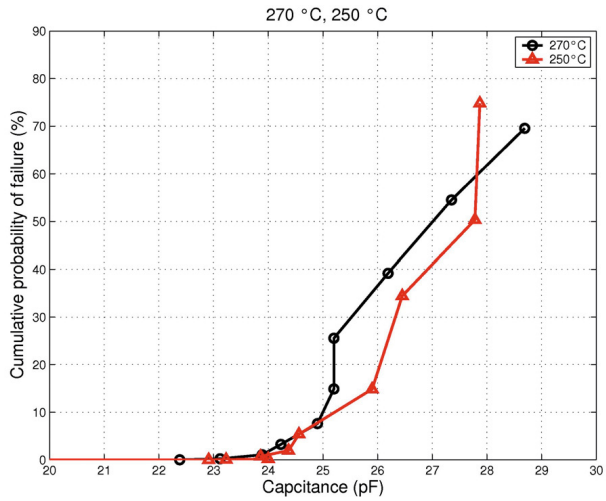

Fig. 3. (Color online) Cumulative probability of failure versus specimen capacitance.

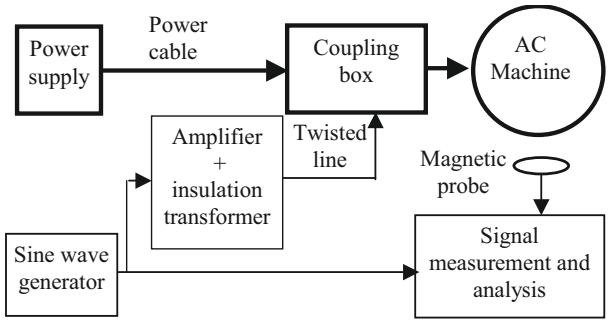

Fig. 4. Block diagram of the proposed monitoring system.

Figure 4 presents the block diagram of the new monitoring system.

The measurement signal is added into the working machine winding with a specially designed coupling box. The variation of the resonance is detected using current measurements but the monitoring system can also work with the low-level external magnetic field. For the first case, the information on insulation aging is global but it is more local in the second case. Figure 5 gives the details of the injection system. Three injection capacitors (Ci) are used as insulation elements for the low frequency power supply, their impedances are high for low frequencies and very low for the injected frequency. The injection inductance (Li) allows to tune the sharp series resonance created by the interaction of the injection inductance and the winding equivalent capacitance, which depends strongly on the turn-to-turn one. The HF test signal is produced by an external sine generator connected to the coupling box by an insulation transformer and a twisted line.

A detailed study of the HF behaviour of the motor winding show that the lower part of the HF impedance spectrum can be modeled by a RLC parallel equivalent circuit [12]. The inductance of this equivalent circuit depends on leakage flux in the machine, the resistance on HF losses and the capacitance is strongly linked to the winding turn-to-turn ones.

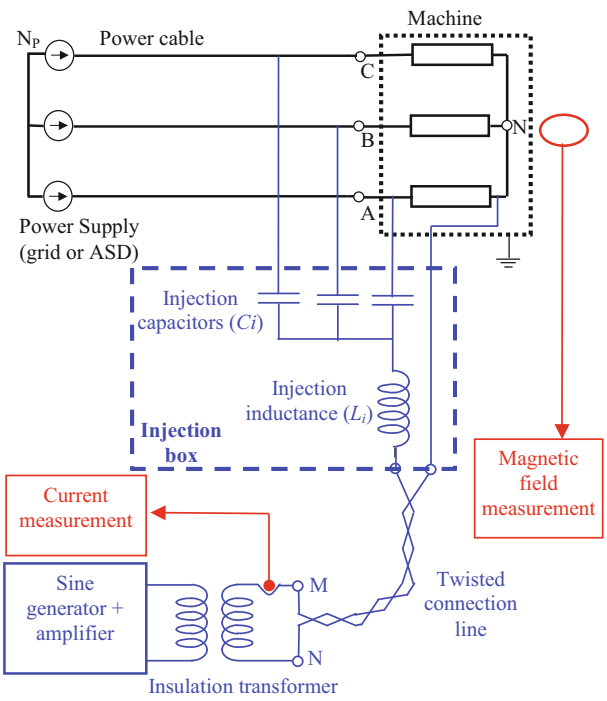

Fig. 5. (Color online) Injection system electric circuit.

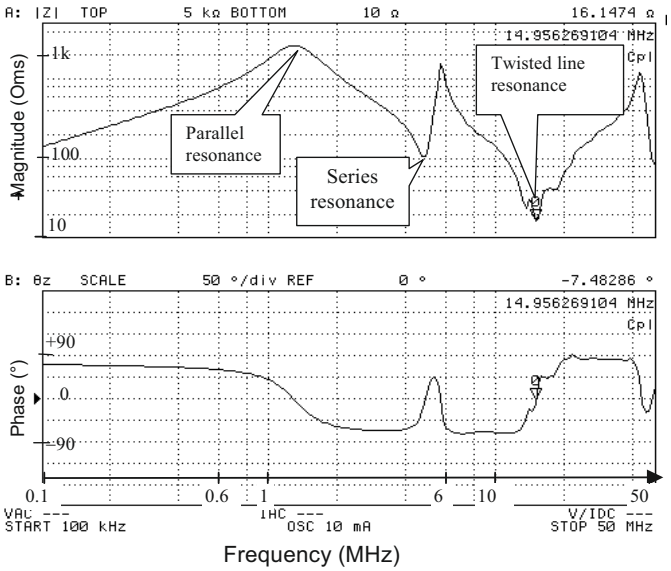

Fig. 6. Impedance of the injection system.

Figure 6 presents the frequency analysis of the whole system including the 4 kW machine, the power cable, the injection box and the twisted line measured with the HP4294A impedance analyzer.

The monitoring system must work at a frequency close to the series resonance pointed out in this figure, which is mainly due to the interaction between the injection inductance Li and the capacitance of the parallel equivalent circuit of the machine. When this capacitance increases, the corresponding series frequency decreases. The measurement method consists in tuning the frequency of the

https://doi.org/10.1051/epjap:2008064 Published online by Cambridge University Press

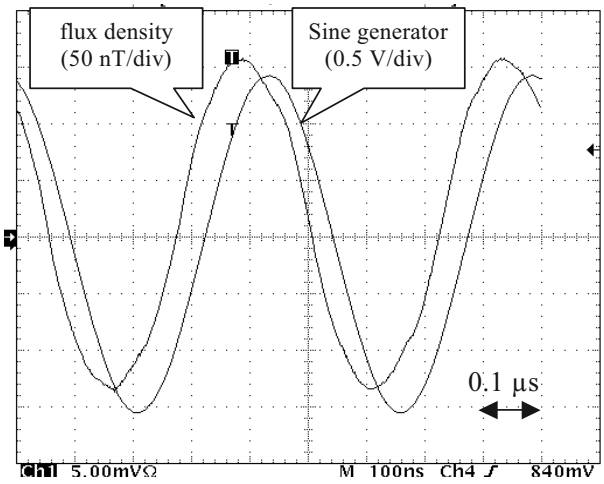

Fig. 7. Injection generator and field probe signals.

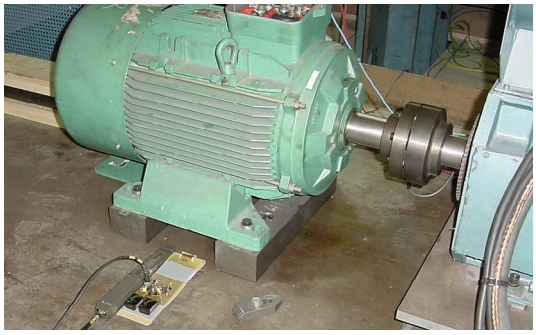

Fig. 8. 45 kW induction machine and magnetic probes.

generator in order to follow the variations of the series resonance frequency. Measurements are performed on the phase: the frequency of the sine generator is tuned in order to get a zero phase lag.

Figure 7 shows the sine wave generator signal and the magnetic flux density measured in the near vicinity of a 4 kW inverter-fed machine for a series resonance close to 2.3 MHz. This figure has been obtained using the averaging of 128 acquisitions of the oscilloscope synchronized by the sine generator. With such a synchronization on an external reference signal, the averaging function acts as synchronous detector that eliminates all the flux density components, which frequency are not multiples of the generator signal frequency. With this method, the flux-density curve is noiseless and it is possible to perform accurate phase measurements on weak fields in a noisy electromagnetic environment.

Other measurements were made on a grid-fed 4-pole 45 kW induction machine. Figure 8 shows the motor and the position of the magnetic probes used for these experiments. Two probes were used: a commercial one (HP11941a) and a less expensive one built in the lab for the useful frequency bandwidth. The aim was to compare measurement in an industrial environment; field measurements were very similar. The injection box was placed on the other side of the machine at a large distance.

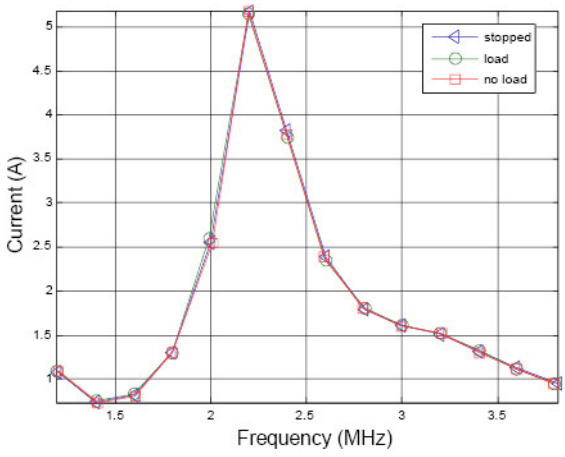

(a)

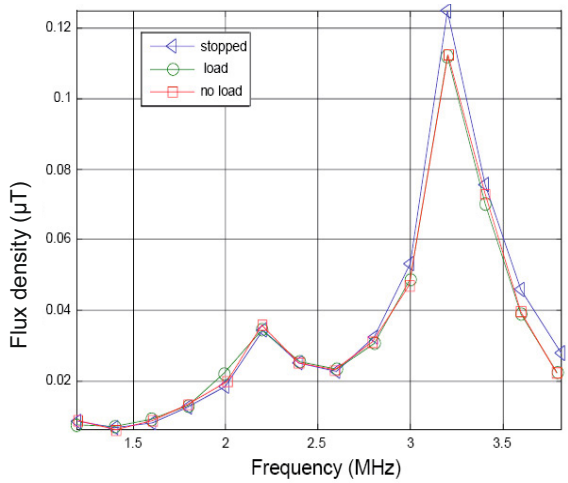

(b)

Fig. 9. (Color online) (a) HF current versus frequency. (b) External flux density versus frequency.

Results are given in Figures 9a and 9b showing respectively the HF current and the flux density versus frequency for three cases: machine stopped, running machine at no load, running machine at full load. The measurement method was the same as for the inverter-fed 4 kW motor. It can be seen that the three curves are nearly superposed for both measurements; the HF behaviour of the machine winding does not depend on the motor mechanical load. The monitoring system is able to work either on a off-line machine or on a running machine.

Figure 9a shows a clear series resonance frequency at 2.2 MHz corresponding to a maximum of the HF current magnitude. The series resonance at 2.2 MHz can be seen on the external flux density curves (Fig. 9b), however a higher maximum at 3.2 MHz can also be observed. This second resonance at a higher frequency can be accounted for by considering local resonances in windings. The stator winding of the experimental 4-pole machine is standard: for each phase, the 4 poles are obtained by connecting in series two set of coils wound on a quarter of the stator

https://doi.org/10.1051/epjap:2008064 Published online by Cambridge University Press

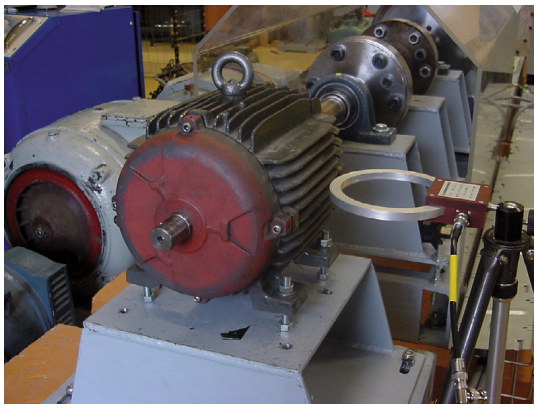

Fig. 10. Induction machine and the flux sensor.

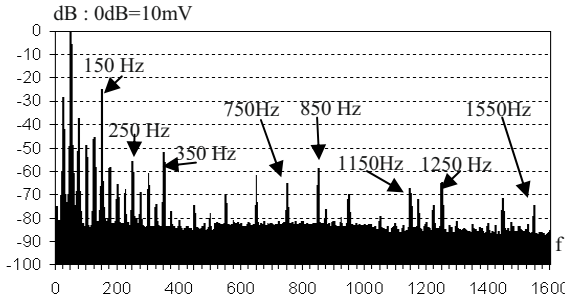

Fig. 11. Flux sensor emf – Intact induction machine.

circumference. The magnetic probes, localized on a side of the machine (Fig. 8), are nearer from a coil than from the second one connected in series and situated on the opposite side of the motor. Magnetic field measurements correspond to more local HF phenomena in windings. Detailed interpretations require a more accurate HF equivalent circuit based on the real winding construction: these HF phenomena depend on slot and end-winding leakage inductances and on turn-to-turn capacitances. The corresponding investigations are now under progress.

3 On-line fault detection

Concerning the analysis of the LF and MF components of the external magnetic field, the study considers the radial field in a plan perpendicular to the machine axis. This field is supposed to be linked to the resulting air-gap flux density b^a, which is obtained by multiplying the air-gap m.m.f. by the per area air-gap permeance. For a 2p-pole machine, b^a can be written as following:

$$b^a = \sum_{K,H} \hat{B}_{K,H} \left(K\omega t - Hp\alpha^s - \varphi_{K,H}\right). \qquad (2)$$

The ranks K, H and the magnitude $\hat{B}_{K,H}$ depend on the supply harmonics, the stator and rotor space harmonics, and the slotting effect. They also depend on the kind of machine (induction or synchronous machine). These harmonic components exist also in the external magnetic field outside the machine but their magnitudes are strongly reduced because of the stator core and the machine housing. It can be shown that the higher H is, the more the flux component is attenuated [13].

The LF and MF components of the external magnetic field are measured by a wound flux sensor set at equal distance from the machine extremities in order to measure only the radial magnetic field (Fig. 10). The frequencies of the spectral lines obtained by a Fourier analysis of the signal delivered by the sensor are directly tied to the rank K. When a fault occurs in the machine, a dissymmetry in the machine structure and/or a change in the currents appear(s). Then, the spectral content of the air-gap flux density is altered: magnitudes change and/or new components appear. This alteration is also visible in the external magnetic field. In that study, turn-to-turn short-circuit faults are considered for an induction and a synchronous machine. Details concerning the modelling of the faults are presented in [14].

3.1 Induction machine

A cage rotor induction machine is considered in that study. This machine, which is widely used in industry has been the object of the major part of the studies on electrical machine diagnosis. Experimental results presented in this paper concern a 11 kW, 4 pole, 50 Hz, 230/400 V induction machine with 32 rotor bars and 48 stator slots. The stator of the machine has been rewound in order to perform stator turn short-circuits.

3.1.1 Intact machine

For an intact machine fed by a balanced 3-phase current system, the development of the air-gap flux density leads to the following expression of K^{IM} and H^{IM}:

$$\left.\begin{aligned} K^{IM} &= k - (h^s - h^r + ksN^s + krN^r)(1-s) \\ H^{IM} &= h^{sr} + k'sN^s + k'rN^r \end{aligned}\right\}. \qquad (3)$$

In these expressions, N^s an N^r are the stator slot and the rotor bar numbers per pole-pair (for the considered machine, $N^s = 24$, $N^r = 16$). h^s and k are equal to $6\nu+1$, with ν a positive, negative or null integer. h^r is an odd positive integer. ks, kr, $k's$ and $k'r$ are integers which vary from $-\infty$ to $+\infty$. h^{sr} can take all the values of h^r and h^s ($h^{sr} = h^s \cup h^r$); s corresponds to the slip.

Figure 11 gives the spectrum of the signal delivered by the flux sensor in a 0–1.6 kHz frequency range when the machine operates at no load ($s \approx 0$). In the lower part of the spectrum ($f < 500$ Hz), the fundamental (50 Hz) can be observed but also harmonics at 150, 250 and 350 Hz which are either generated by the supply (rank k of Eq. (3)) or due to the magnetic saturation. This latter, which deforms the air-gap flux density and modifies its spectral content, is however not taken into account in the modelling of the machine that leads to define the ranks given by (3). In the MF range, the spectral

https://doi.org/10.1051/epjap:2008064 Published online by Cambridge University Press

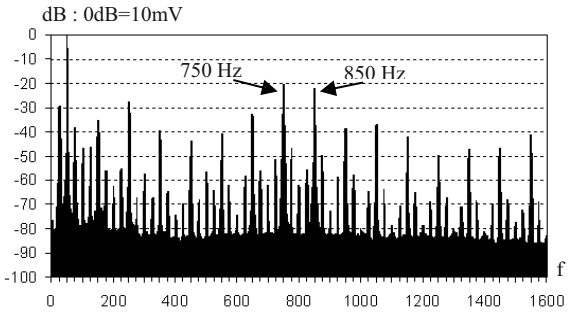

Fig. 12. Flux sensor emf – Induction machine with stator winding short-circuit fault.

lines tied to the slotting effects appear. These ones tied to the rotor have the following frequencies: 750, 850 and 1550 Hz. They correspond to $k = 1$ $h^s = h^r$, $ks = 0$, $kr = \pm 1$ and $kr = 2$ in the definition of K^{IM} in (3). In this frequency range, spectral lines at 1150 and 1250 Hz also appear, they are linked to the stator slotting spectral lines and they are obtained for $k = 1$, $h^s = h^r$, $kr = 0$, $ks = \pm 1$ in (3). Let us point out that the derivative effect of the sensor amplifies the MF components, that enhance the slotting spectral lines.

3.1.2 Stator turn-to-turn short circuit fault

The degradation of the winding insulation is an inescapable phenomenon during the operation of the machine. The ultimate point of the degradation is a rupture of the insulation, generating a contact between several stator turns. The short-circuited turns are flowed through by a high induced current which generates a local heating of the winding. Then the short-circuit can spread to all the winding. In some cases, the impedance of the shorted turns is such that the short circuit current is limited, and the winding can support the temperature. Then, the fault can stay without any visible symptom, but in this case, faster aging of the insulation precedes further deterioration of the winding. Detection techniques of that faults exist, they mainly use the current measurement [15,16]. The interest of the use of the external magnetic field for diagnosis is that the induced short-circuit current contributes to it. So the sensitivity to the fault is higher than in the line current. It is also shown in [14] that the induced short-circuit current makes a change in spectral lines defined by the following ranks:

$$K_{ssc}^{IM} = k - \left(\frac{h}{p} - h^r + ksN^s + krN^r\right)(1 - s), \qquad (4)$$

k and h^r can take all positive integer values. h, ks and kr vary from $-\infty$ to $+\infty$ (but h is different from 0). Figure 12 gives the spectrum of the signal delivered by the flux sensor when 12.5% of the phase 1 winding is short-circuited, with the short-circuit current limited to 20 A. The machine still operates at no load ($s \approx 0$).

It can be noticed that the spectral lines at 750 and 850 Hz are very sensitive to the fault, they correspond to the rotor slotting effect and they can be obtained with $k = 1$, $kr = \pm 1$, $h = ph^r$, $ks = 0$ in (4). It also appears sideband spectral lines at ± 25 Hz on the whole spectrum. It is essentially due to the h/p term in (4) and it actually traduces the reaction of the rotor cage to the fault.

3.2 Synchronous machine

The interest for the diagnostic of this kind of machine in low and medium power applications has increased because of development of applications in the field of transport or wind-turbines. Different kinds of synchronous machines exist, they differ only from the structure of their rotor: wound salient or wound smooth rotor (turbo alternator), surface mounted or interior permanent magnet rotor. The modelling of the intact synchronous machine and the faulty one is deduced from the induction machine study. Actually, the stator has the same structure for the both machine, and it will be considered that the rotor saliency of the synchronous machine is similar to the rotor slot effect of an induction machine whatever the rotor structure. Moreover, the secondary slotting effect due to the dampers, which can possibly exist, will be neglected. Consequently, as the number of rotor saliencies is equal to the pole number of the machine, the frequency ranks given by (3) and (4) can be considered again in the case of a synchronous machine, with $N^r = 2$ and $s = 0$.

The experiments are realized on a 11 kW, 230/400 V, 50 Hz, 4 salient pole synchronous machine, with $N^s = 18$. The machine has been rewound at the stator and at the rotor, that allows one to short-circuit a part of the stator or the rotor windings.

3.2.1 Intact machine

In the case of an intact synchronous machine, one can define the rank K^{SM} and H^{SM} as following:

$$\left.\begin{aligned} K^{SM} &= k - (h^s - h^r + ksN^s + 2kr) \\ H^{SM} &= h^{sr} + k'sN^s + 2k'r \end{aligned}\right\}. \qquad (5)$$

The variations of the different parameters are the same as those given in 3.1.1 for the induction machine. The ranks given by (5) take the damper effects into account, although the reluctance effect of the dampers is neglected [17]. Figure 13 gives the spectrum of the signal delivered by the flux sensor when the machine is supplied by the grid and operates as a motor at no load. Comparatively to the induction machine, the spectral lines related to the rotor slotting effect do not appear so clearly. The reason is that these spectral lines are located in LF. For example, considering $k = 1$, $h^s = h^r$, $ks = 0$, $kr = \pm 1$ in the expression of K^{SM} given in (5) leads to 50 Hz which also corresponds to the fundamental component and the 150 Hz component which can be attributed to the saturation phenomenon. Moreover, the other rotor slotting spectral lines ($kr = \pm 2$, $kr = \pm 3 \ldots$) are merged by twins at 150 Hz, 250 Hz, 350 Hz, ... Concerning the stator slotting spectral lines ($k = 1$, $h^s = h^r$, $kr = 0$, $ks = \pm 1$), they clearly appear at 850 and 950 Hz.

https://doi.org/10.1051/epjap:2008064 Published online by Cambridge University Press

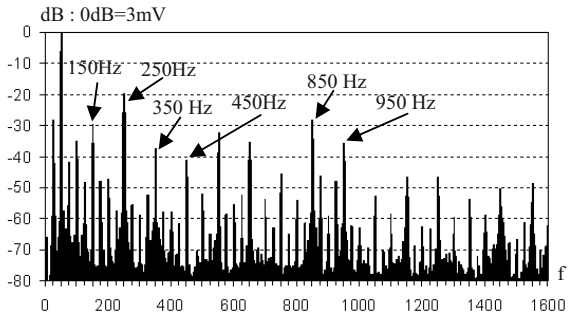

Fig. 13. Flux sensor emf – Intact synchronous machine.

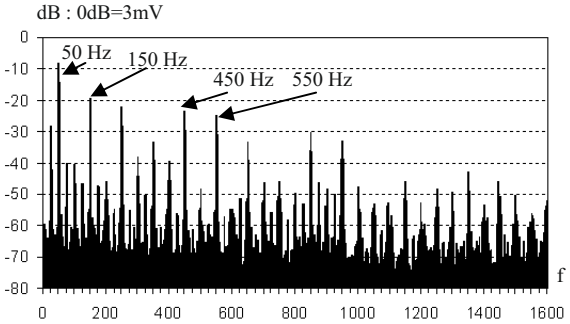

Fig. 14. Flux sensor emf – Synchronous machine with stator winding short-circuit fault.

3.2.2 Stator turn-to-turn short circuit

The typical ranks of the fault are deduced from these given for the induction machine. They are defined thanks to (4) with the same variation of the parameters [17]:

$$K_{ssc}^{SM} = k - \left(\frac{h}{p} - h^r + ksN^s + 2kr\right) \cdot \qquad (6)$$

Figure 14 gives the spectrum of the signal delivered by the flux sensor when 16% of the winding of one phase is short-circuited with the short-circuit current limited to 20 A. It can be observed that the rotor slotting spectral lines are not so sensitive than for the induction machine. The reason, as exposed for the intact machine, is that the sensitive spectral lines are merged with non negligible other spectral lines. For instance, it appears that the fundamental at 50 Hz decrease of 9 dB, whereas the 150 Hz increase of 10 dB when the fault occurs. So the first rotor spectral lines ($kr = \pm 1$ in (6)) are not good indicators of the fault. It can be observed that the most sensitive spectral lines appear for higher rank: $kr = \pm 4$ (350 Hz, 450 Hz). Contrary to the case of induction machine, sideband frequencies at $\pm$fr (due to the term h/p) do not appear with the fault. It means that the rotor has no reaction to the fault. The external magnetic field still gives information about stator turn-to-turn short-circuit in synchronous machines but the investigation area in the spectrum must be wider than for induction machine.

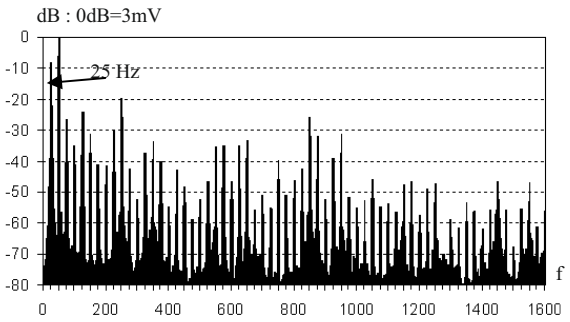

Fig. 15. Flux sensor emf – Synchronous machine with rotor winding short-circuit fault.

3.2.3 Rotor turn-to-turn fault

The rotor turn-to-turn failure, which concerns wound rotor synchronous machines, can exist without important thermal stress because, as the rotor rotates at the synchronous speed, no induced current at the fundamental frequency exists in the shorted turns. However, the machine performances decrease, due to an alteration of the back emf. The dissymmetry produced by the fault and the induced harmonic currents which flow in the shorted turns generate additional air-gap flux density components which will be refund in the external radial magnetic field. It is shown in [17] that their frequency ranks are defined as following:

$$K_{rsc}^{MS} = k - h^s + \frac{h}{p} + ksN^s + 2kr, \qquad (7)$$

k varies from 1 to $+\infty$, h, ks and kr vary from $-\infty$ to $+\infty$. h^s is equal to $6\nu + 1$, with ν a positive, negative or null integer. Figure 15 gives the spectrum of the sensor emf when 12.5% of the rotor winding is short-circuited. One can observe a high magnitude of the 25 Hz component, obtained by equation (7) with $k = h^s$, $ks = kr = 0$, $h = 1$. It can also be observed high magnitude side band spectral lines at $\pm$25 Hz around the whole lines of the spectrum, they result from the h/p terms in (7). The high sensitivity to the fault of spectral lines defined by (7) makes it possible to expect again a good sensitivity for incipient rotor faults.

4 Conclusion

The insulation aging modifies the turn-to-turn capacitance and changes the HF resonances of the motor winding. With the appropriate injection system, this phenomenon is detectable on the HF components of the electromagnetic emissions. On the other hand, a turn-to-turn short-circuit fault in the machine modifies the mmf. and also the currents in the stator and (or) rotor windings. In that case, the low and medium spectral content of the external magnetic field is altered, and the fault can be detected. The presented study shows that the health of an electrical machine can be evaluated with a non-invasive

https://doi.org/10.1051/epjap:2008064 Published online by Cambridge University Press

method, by only the measurement of the external magnetic field. The valuation goes from the insulation testing to the fault detection. The method can be implemented on induction or synchronous machines fed with the grid or with an inverter.

This work in supported by the program "Futurelec 2" supervised by the French National Center of Technological Research (CNRT) on electrical engineering. This program, including *EDF* and *Framatome ANP*, is sponsored by the *region Nord Pas-de-Calais* (France), the French ministry (FRT) and the European funds (FEDER).

References

1. L. Schmerber, L.L. Rouve, A. Foggia, *IEMDC 2005 Conference, May 2005, San Antonio, Texas (USA)*, pp. 92–98
2. P. Ferrari, A. Mariscotti, A. Motta, P. Pozzobon, IEEE Trans. Energy Convers. **16**, 68 (2001)
3. R.M. Tallam et al., *Symposium on Diagnostics for Electric machines, Power Electronics and Drives, SDEMPED, Atlanta, USA, 24–26 August 2003*, pp. 35–46
4. M. Fenger, S.R. Campbell, J. Pedersen, IEEE Ind. Appl. Mag. (July/August 2003), pp. 22–31
5. G.C. Stone, E.A. Boulter, I. Culbert, H. Dhirani, Electrical Insulation for Rotating Machines, IEEE Press Series Power Eng. (2004)
6. E. Wiedenbrug, G. Frey, J. Wilson, *Pulp and paper industry Technical Conference, 16–20 June 2003*, pp. 50–55
7. A. Cavalini, G.C. Montanari, F. Puletti, A. Contin, IEEE Trans. Dielect. Elect. Insul. **12**, 203 (2005)
8. C. Hudon, N. Amyot, T. Lebey, P. Castelan, N. Kandev, IEEE Trans. Dielect. Elect. Insul. **7**, 783 (2000)
9. P. Werinski, Ph.D. thesis, University of Artois, July 2006
10. P. Werynski, D. Roger, R. Corton, J.F. Brudny, IEEE Trans. Energy Convers. **21**, 673 (2006)
11. J.C. Fothergill, L.A. Dissado, *Electrical Degradation and Breakdown in Polymers* (Peter Peregrinus, IEE, 1992)
12. F. Perisse, P. Werynski, D. Roger, IEEE Trans. Dielect. Elect. Insul. Syst. **14**, 1308 (2007)
13. D. Thailly, R. Romary, J.F. Brudny, *16th International Conference on Electrical Machines, ICEM 2004*, Résumé, pp. 781–782, Article: CD ROM, paper No. 707
14. R. Romary, R. Corton, D. Thailly, J.F. Brudny, Eur. Phys. J. Appl. Phys. **32**, 125 (2005)
15. W.T. Thomson, M. Fenger, IEEE Ind. Appl. Mag. **7**, 26 (2001)
16. A. Stavrou, H.G. Seddings, J. Penman, IEEE Trans. Energy Convers. **16**, 32 (2001)
17. D. Thailly, R. Romary, J.Ph. Lecointe, J.F. Brudny, P. Suau, *17th International Conference on Electrical Machines, ICEM 2006*, Résumé, p. 59, Article: CD ROM, paper No. 462